Membrane Technology
ISSN (online): 1873-4049

Energy Method for Analyzing the Large Deformation of Geogrid Cushions Above Cylindrical Soil Cavities

Xiangru Yang[1,2]

1.Fujian Chuanzheng Communications College, Fuzhou, China
2.Fujian Chuanzheng Communications Management Co., Ltd, Fuzhou, China

Abstract:
In regions prone to soil cavity development, geogrid-reinforced embankments must consider the impact of foundation settlement. This study models the geogrid cushion as a thin circular elastic plate, with the embankment's self-weight, vehicular traffic loads, and the frictional forces at the reinforcement-soil interface all translated into external loads. Utilizing the Pasternak model to simulate the foundation, we adhere to the principle of large deflection in thin plates to account for three types of strain energy and the work done by external loads, thereby deriving analytical expressions for the deformation of the geogrid cushion. We analysed the impact of embankment height, reinforcement-soil interface parameters, modulus of subgrade reaction, and the shear modulus of the foundation soil on the deflection of the reinforced-cushion. The findings reveal that when the embankment height surpasses the cavity diameter, its influence on differential settlement in anchorage areas becomes negligible. As the tangential resistance coefficient at the reinforcement-soil interface increases, its effect on differential settlement in the subsidence area progressively diminishes. The modulus of subgrade reaction influences differential settlement in anchorage areas but not in the collapsed area. The taller the embankment, the more significant the impact of the modulus of subgrade reaction in the collapsed area. When the embankment height and the thickness of the Pasternak shear layer are considerable, and the modulus of subgrade reaction is low, the effect of the foundation shear modulus on the deflection of the reinforced-cushion must be considered.

Keywords: Cavity, geogrid cushion, energy method, large deformation, Pasternak foundation.

INTRODUCTION

With the swift expansion of infrastructure and the dwindling availability of developable land, an increasing number of structures—municipal roads, highways, and railroads—are being constructed in karst regions[1]. To ensure the ongoing functionality of these structures despite cavity formation, various foundation treatments, such as piles and geosynthetics, are frequently implemented. Among the myriads of reinforcement options, geosynthetics are favoured for their time efficiency, cost-effectiveness, environmental sustainability, and user-friendliness [2]. Geosynthetics, which serve to bridge potential voids beneath load-bearing granular layers, encompass woven geotextiles, geogrids, and geocomposites [3,4].

Current research on geosynthetics spanning cavities primarily examines the interplay between geosynthetics, embankment materials, and sinkholes. The influence of foundation deformation on the reinforced cushion is predominantly manifested through friction at the reinforcement-soil interface. Giroud et al. (1990) [5] and Wang et al. (1996) [6] developed a method for calculating the tensile force of geosynthetics in collapsed areas, presupposing that the reinforcement material remains undeformed outside the cavity. Subsequent studies by Briancon & Villard (2008) [7], Villard & Briancon (2008) [8], Le et al. (2014) [9], Van & Jacobsz (2016) [10], Villard et al. (2016) [2], Huckert et al. (2016) [11], Lai (2018) [12], and Wang et al. (2024) [13] focused on the load-bearing and deformation behaviour of the reinforcement outside the cavity. Employing a variety of methods, including theoretical analysis, numerical simulation, and prototype or model testing, these studies elucidated the stress-deformation behaviour of geosynthetics in both anchorage and collapsed areas. However, these studies did not treat the foundation, sinkholes, and reinforced cushion as an integrated system, nor did they explore the impact of foundation settlement in anchorage areas on the deformation of the reinforced embankment. In practice, under the load of backfill and traffic or due to groundwater fluctuations, foundations may not only develop voids but also experience settlement.

Research on foundation-reinforced embankments predominantly centres on pile-supported embankments and those over soft foundations [14]. Typically, soil-structure interaction is modelled as a beam-soil interaction system [15-20]. For foundation-soil analysis, Pasternak introduced a two-parameter foundation model that builds upon the Winkler model by incorporating the effects of transverse shear deformation, thereby broadening its applicability [21]. The challenge of geosynthetics in continuous foundations is often reduced to a Timoshenko beam model [15- 17] or a Euler-Bernoulli beam model [18-20]. These beam-soil system methods, predicated on plane strain, are grossly inaccurate for karst regions. Given that the geosynthetic's planar dimensions significantly exceed those of sinkholes, employing the large deflection analysis of circular elastic plates to simulate the geogrid structural layer above a cylindrical cavity is more rational.

Güler (2004) [22] and Shukla et al. (2011) [23] independently applied the Galerkin and Ritz methods to investigate a thin circular elastic plate on a Pasternak foundation under a concentrated central load. These analytical methods, predicated on small deformations, are unsuitable for analysing the large-scale deformations of geosynthetics over sinkholes.

Drawing on the von-Kármán theory, Jones et al. (2010) [24] utilized a three-dimensional thin plate model to simulate geosynthetics in a pile-supported embankment on soft soil. For composite foundations, comprising a geogrid cushion over gravel piles, Zhao et al. (2016) [25] employed a thin flexible plate capable of large deflections to simulate the geogrid's bending resistance. This research suggests that thin flexible plate theory is a viable approach to study geogrid cushion deformation.

However, the strong interaction between the foundation, sinkhole, and geogrid cushion, coupled with their coordinated deformation, renders the relationships among these three components highly complex. In our calculations, the foundation, sinkhole, and geogrid cushion are treated holistically, with the overburden fill's self-weight, traffic loading, and soil-reinforcement frictional forces all converted into external loads. Based on the principle of minimum potential energy, under the influence of backfill and vehicular traffic, there exists a set of displacements that meet the displacement boundary conditions and minimize the total potential energy to zero.

In this study, the energy method was employed to thoroughly account for three types of strain energy—related to the bending of thin plates, mid-plane deformation, and Pasternak foundation deformation—as well as the work associated with the embankment's self-weight, vehicular traffic loading, and soil-reinforcement interface friction. We propose a method to address the deformation of the reinforced cushion, factoring in foundation deformation in areas where sinkholes develop.

ENERGY METHOD FOR DEFORMATION CALCULATIONS

Analytical Model

For embankments reinforced over cylindrical cavities, the geogrid cushion is modelled as a thin circular elastic plate, with the Pasternak model utilized to characterize the foundation soil. The soil-arching effect results in distinct stress conditions within the geogrid cushion between the collapsed area and the anchorage zones.

The analysis is predicated on several key assumptions:

1. The calculation omits the increased pressure on the geogrid cushion near the sinkhole in the anchorage areas, an outcome of the earth pressure redistribution in the collapsed area. Adachi et al. (2003) [26] observed in three-dimensional experiments that all four sides can resist the heightened earth pressure due to the descending trapdoor, with the maximum compressive stress increment in the anchorage section being 0.1-0.2 times the original pressure.

2. The loads exerted on the geogrid cushion in both the collapsed area and the anchorage areas are presumed to be uniformly distributed.

3. The variation in strength of the reinforcing material across the horizontal plane is not taken into account.

4. It is assumed that the mid-plane of the geogrid cushion, which is normal to the cushion, remains straight both pre- and post-deformation.

5. The thickness of the geogrid cushion is considered constant throughout the deformation process.

6. The geogrid cushion, embankments, and the underlying foundation are assumed to be intact and to maintain an elastic state before and after deformation.

7. The geogrid cushion is assumed to exhibit isotropic properties in both longitudinal and transverse directions.

In the analytical model, the centre of the collapsed area is designated as point O, as depicted in Figure 1. The model is asymmetric, with point A marking the edge of the soil cavity and point B defining the influence boundary of the soil cavity collapse (a fixed boundary). In Figure 1, a represents the radius of the cavity (m), b represents the radius of influence of the cavity (m), w represents deflection (m), q_0 represents the load applied on anchorage areas (kPa), n represents the coefficient related to soil arching effect (dimensionless).

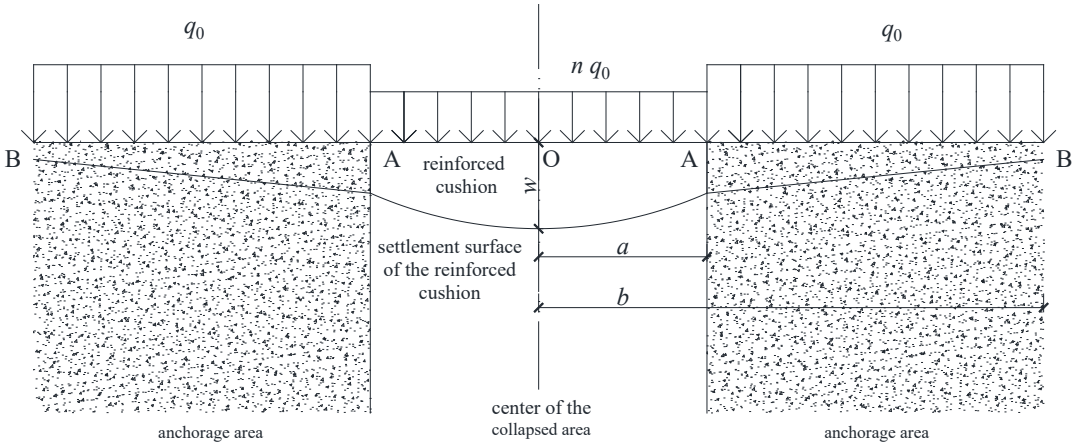

Figure 1. Analytical model

Energy Equation

Drawing upon the theory of thin flexible plates that account for large deflections, the curvature strain energy of the reinforced cushion is articulated as follows:

$$W = \pi D \int \left(\rho \left(\frac{d^2 w}{d\rho^2} \right)^2 + \frac{1}{\rho} \left(\frac{dw}{d\rho} \right)^2 + 2\mu \frac{dw}{d\rho} \frac{d^2 w}{d\rho^2} \right) d\rho \tag{1}$$

W - coefficient related to soil arching effect (dimensionless);

D - flexural rigidity of the reinforced-cushion (kN·m), $D = \frac{E\delta^3}{12\left(1-\mu^2\right)}$;

ρ - radial distance of the point from the cavity centre (m);

μ - poisson's ratio of the reinforced-cushion (dimensionless);

E - elastic modulus of reinforced-cushion (kN/m^2);

δ - reinforced-cushion thickness (m).

The strain energy due to the mid-plane deformation of the geogrid cushion is expressed as:

$$U = \frac{\pi E \delta}{1-\mu^2} \int \left(\left(\frac{du}{d\rho} + \frac{1}{2} \left(\frac{dw}{d\rho} \right)^2 \right)^2 + \frac{u^2}{\rho^2} + 2\mu \frac{u}{\rho} \left(\frac{du}{d\rho} + \frac{1}{2} \left(\frac{dw}{d\rho} \right)^2 \right) \right) \rho d\rho \tag{2}$$

The load exerted on the Pasternak foundation, denoted as $q = k_s w - GH\left(\frac{d^2 w}{d\rho^2} + \frac{1}{\rho} \frac{dw}{d\rho} \right)$ [23], influences the strain energy associated with the foundation's deflection, which can be articulated as follows:

$$K = 2\pi \int \frac{1}{2} q w \rho d\rho = \pi \int \left(k_s w - GH \left(\frac{d^2 w}{d\rho^2} + \frac{1}{\rho} \frac{dw}{d\rho} \right) \right) w \rho d\rho \tag{3}$$

q - load applied on the foundation (kPa);

k_s - modulus of subgrade reaction of the Pasternak foundation (kN/m^3);

G - shear modulus of the Pasternak foundation (kN/m^2);

H - thickness of the Pasternak shear layer (m);

K - strain energy associated with the foundation deflection (kJ).

The external work encompasses both the contributions from vertical loads, such as the self-weight of the embankment and traffic loading, as well as horizontal loads, namely the frictional forces at the reinforcement-soil interface. This external work can be mathematically expressed as:

$$Q = 2\pi\int\left(qw - k_h u^2\right)\rho d\rho \tag{4}$$

Q - work done by load q (kJ);

k_h - tangential resistance coefficient of reinforced cushion interface (kN/m^3), $k_h = \frac{\tau_{\max}}{u_{\min}}$;

$\tau_{\max}$ - maximum frictional resistance of the reinforcement-soil interface (kPa);

$u_{\min}$ - minimal displacement for maximal friction mobilization (m).

Displacement Boundary Conditions

For $\rho=b$, $w(b)=\frac{q_0}{k_s}$, $\frac{dw}{d\rho}|_{\rho=b}=0$, $\frac{d^2w}{d\rho^2}|_{\rho=b}=0$, $u(b)=0$, $\varepsilon_\rho(b)=\left(\frac{du}{d\rho}+\frac{1}{2}\left(\frac{dw}{d\rho}\right)^2\right)\Big|_{\rho=b}=0$.

Where $q_0=\gamma(h+h')$. γ represents the unit weight of the soil (kN/m^3), h represents the embankment height (m); h' represents the height of the equivalent soil column that corresponds to the excess load on the ground surface.

For $\rho=0$, $u(0)=0$, $\frac{dw}{d\rho}|_{\rho=0}=0$.

According to Huckert et al. (2016) [11], Villard et al. (2016) [2], Lai (2018) [12], b = 4a, radial strain of reinforcement is close to 0. So the analysis range is 4 times of the radius of the sinkhole. Because point B is fixed with multiple boundary conditions, the analysis starts from the AB segment.

Displacement Function Definition

Scholars, through moving trapdoor experiments and numerical analysis, have identified various types of deflection curves for geosynthetics in the collapsed area. These include the catenary curve as described by Blight & Barrett (1990) [27], the hyperbolic curve reported by Le et al. (2014) [9], and the parabolic curve documented by Espinoza & Bray (1995) [28]and He et al. (2016) [29].

Utilizing the Ritz method, the deformations within the AB segment are specified as follows:

$$w_1[\rho] = C_1\left(1-\frac{\rho^2}{b^2}\right)^2+\frac{q_0}{k_s} \tag{5}$$

$$u_1[\rho] = \left(A_1+A_2\frac{\rho}{b}\right)\left(1-\frac{\rho}{b}\right)^3 \tag{6}$$

The deformations of the OA segment are expressed as:

$$w_2[\rho] = C_2\left(1-\frac{\rho^2}{a^2}\right)+C_1\left(1-\frac{a^2}{b^2}\right)^2+\frac{q_0}{k_s} \tag{7}$$

$$u_2[\rho] = \frac{\rho}{a}\left(1-\frac{\rho}{a}\right)\left(A_3+A_4\frac{\rho}{a}\right)+\rho\left(A_1+A_2\frac{a}{b}\right)\left(1-\frac{a}{b}\right)^3 \tag{8}$$

The coefficients A_1, A_2, A_3, A_4, C_1, and C_2 are mutually independent.

Considering nondimensional parameters as: $b^*=\frac{b}{a}=4$, $\rho^*=\frac{\rho}{a}$, $\delta^*=\frac{\delta}{a}$, $w^*=\frac{w}{a}$, $u^*=\frac{u}{a}$, $h^*=\frac{h}{a}$, $h'^*=\frac{h'}{a}$,

$\gamma^* = \frac{\gamma a^4}{D}$, $q_0^* = \frac{q_0 a^3}{D}$, $k_h^* = \frac{k_h a^4}{D}$, $k_s^* = \frac{k_s a^4}{D}$, $G^* = \frac{Ga^3}{D}$, $H^* = \frac{H}{a}$, $C_i^* = \frac{C_i}{a}$ （i=1, 2）, $A_j^* = \frac{A_j}{a}$ （j=1, 2, 3,4）, $W^* = \frac{W}{\pi D}$, $U^* = \frac{U}{\pi D}$, $K^* = \frac{K}{\pi D}$, $Q^* = \frac{Q}{\pi D}$.

Eqs.(5)–(8) are transformed into:

$$w_1^*\left[\rho^*\right] = C_1^*\left(1-\left(\frac{\rho^*}{4}\right)^2\right)^2 + \frac{q_0^*}{k_s^*} \tag{9}$$

$$u_1^*\left[\rho^*\right] = \left(1-\frac{\rho^*}{4}\right)^3\left(A_1^* + \frac{\rho^* A_2^*}{4}\right) \tag{10}$$

$$w_2^*\left[\rho^*\right] = C_2^*\left(1-\rho^{*2}\right) + w_1^*\left[\rho^*\right] = C_2^*\left(1-\rho^{*2}\right) + 0.879C_1^* + \frac{q_0^*}{k_s^*} \tag{11}$$

$$u_2^*\left[\rho^*\right] = \rho^*\left(1-\rho^*\right)\left(A_3^* + A_4^*\rho^*\right) + u_1^*\left[\rho^*\right] = \rho^*\left(1-\rho^*\right)\left(A_3^* + A_4^*\rho^*\right) + 0.422\rho^*\left(A_1^* + \frac{A_2^*}{4}\right) \tag{12}$$

Displacement Equation Solution

Within the AB segment, the energy equations are formulated as follows:

$$W_1^* = 0.612C_1^{*2} - 0.0549\mu C_1^{*2} \tag{13}$$

$$\begin{aligned} U_1^* = \frac{1}{\delta^{*2}}\Big(&(2.62-2.14\mu)A_1^{*2} + (1.25-1.07\mu)A_1^*A_2^* + (0.208-0.133\mu)A_2^{*2} \\ &+ (0.388\mu-1)A_1^*C_1^{*2} + (0.166\mu-0.337)A_2^*C_1^{*2} + 0.227C_1^{*4}\Big) \end{aligned} \tag{14}$$

$$K_1^* = 0.446G^*H^*C_1^{*2} + 1.16C_1^{*2}k_s^* + 4.39C_1^*q_0^* + \frac{7.5q_0^{*2} - 0.234G^*H^*C_1^*q_0^*}{k_s^*} \tag{15}$$

$$Q_1^* = -k_h^*\left(0.21A_1^{2*} + 0.153A_1^*A_2^* + 0.0296A_2^{2*}\right) + 4.39C_1^*q_0^* + \frac{15q_0^{*2}}{k_s^*} \tag{16}$$

In the OA segment, the energy equations are articulated as:

$$W_2^* = 4C_2^{*2}(1+\mu) \tag{17}$$

$$\begin{aligned} U_2^* = \frac{1}{\delta^{*2}}\Big(&(1+\mu)\left(2.14A_1^{*2} + 1.07A_1^*A_2^* + 0.133A_2^{*2} + 5.06A_1^*C_2^{*2} + 1.27A_2^*C_2^{*2}\right) \\ &+ C_2^{*2}(\mu-3)\left(2.4A_3^* + 1.6A_4^*\right) + 3A_3^{*2} + 3.6A_3^*A_4^* + 1.4A_4^{*2} + 8C_2^{*4}\Big) \end{aligned} \tag{18}$$

$$K_2^* = 0 \tag{19}$$

$$\begin{aligned} Q_2^* = -k_h^*\Big(&0.089A_1^{*2} + 0.0445A_1^*A_2^* + 0.00556A_2^{*2} + 0.0844A_1^*A_3^* + 0.0211A_2^*A_3^* + 0.0333A_3^{*2} \\ &+ 0.0563A_1^*A_4^* + 0.0141A_2^*A_4^* + 0.0381A_3^*A_4^* + 0.0119A_4^{*2}\Big) + 0.879nC_1^*q_0^* + 0.5nC_2^*q_0^* + \frac{nq_0^{*2}}{k_s^*} \end{aligned} \tag{20}$$

The coefficient n is associated with the soil arching effect. Drawing from Terzaghi's theory on the soil-arching effect as elaborated [5], $n = \frac{\sigma_v}{q_0}$; $\sigma_v = \frac{\gamma a - 2c}{2K_0\tan\varphi}\left(1-e^{-2K_0(h/a)\tan\varphi}\right) + \gamma h' e^{-2K_0(h/a)\tan\varphi}$; $K_0 = 1-\sin\varphi$.

In there, σ_v - vertical stress in collapsed area (kPa);

K_0 - coefficient of earth pressure at rest (dimensionless);

c - fill material cohesion, geosynthetic and overlying fill cohesion;

φ - internal friction angle of fill material.

In the analysis, the geogrid cushion, the underlying cavity, and the foundation are considered as a single integrated system. The total potential deformation energy encompasses both the potential energy of the entire system and the potential energy exerted by external forces.

$$\Pi^* = \left(W_1^* + U_1^* + K_1^* - Q_1^*\right) + \left(W_2^* + U_2^* + K_2^* - Q_2^*\right) \tag{21}$$

$$\Pi^* = \Pi^*\left[\mu, \delta^*, n, q_0^*, k_{hu}^*, k_{hl}^*, k_s^*, G^* H^*\right]$$

Π-total potential energy(kJ), Π^* is dimensionless.

Employing the principle of minimum potential energy, the coefficients A_1^*, A_2^*, A_3^*, A_4^*, C_1^*, and C_2^* can be ascertained through Eqs. (22) and (23).

$$\frac{\partial \Pi^*}{\partial A_i} = 0 \quad (i = 1,2,3,4) \tag{1}$$

$$\frac{\partial \Pi^*}{\partial C_j} = 0 \quad (j = 1,2) \tag{2}$$

SOLUTION VERIFICATION

In their study on cylindrical cavities, Huckert et al. (2016) [11] investigated the load transfer mechanisms in geotextile-reinforced embankments. They employed horizontal double-layered coaxial inflatable tubes placed within a foundation cavity to simulate the progressive expansion of the cavity under natural conditions by releasing gas. Concurrently, they measured the deformations of the geotextile during the cavity formation process. Building upon Huckert's test conditions, Villard et al. (2016) [2] utilized a discrete-element model to simulate geotextile deformation under two scenarios: gradual cavity formation (proc A) and rapid cavity formation (proc B). Lai (2018) [12] examined the load transfer mechanism of low-filled reinforced road subgrade against cavity collapse, based on partial soil-arching, and derived the geotextile deformation through theoretical calculations. However, in the aforementioned analyses, including experiments and both numerical and theoretical calculations, foundation deformation was not taken into account. For ease of comparison, the deformation of the foundation outside the void was neglected, implying that w1=0. The strain energy related to foundation deflection K=0. The properties of geotextiles differ significantly from those of elastic thin plates but are more analogous to thin films. Given this, the flexural rigidity of the geotextile is considered negligible, resulting in the absence of curvature strain energy within the reinforced-cushion. So, $\Pi = \left(U_1 - Q_1\right) + \left(U_2 - Q_2\right)$.

The experimental and computational parameters are presented in Table 1.

Table 1. Prototype test and calculation parameters

Material	Properties
Embankment fill	γ=15.6kN/m^3, φ=36°, c=0, h=1m, $h'=0$, n=0.771
Geotextile	φ_u=23°, φ_l=40°, $c_u = c_l = 0$, $\mu = 0.35$, δ=0.003m, k_h=1300kN/m^3, J=2988 kN/m, E=400MPa*
Cavity	a=1.1m, b=4.4m

*φ_u - internal friction angle between the geosynthetic and the overlying fill (°);

φ_l - internal friction angle between the geosynthetic and the underlying fill (°);

c_u - geosynthetic and overlying fill cohesion (kPa);

c_l - geosynthetic and underlying fill cohesion (kPa);

J - tensile stiffness per unit width of the geosynthetic fabric (kN/m).

Verification of Reinforced-Cushion Deflection

Based on the preceding analysis, the equations that describe the settlement curve of the reinforced-cushion are detailed below:

$$\begin{cases} w_1[\rho] = 0 & 1.1 < \rho \le 4.4 \\ w_2[\rho] = 0.199 - 0.164\rho^2 & 0 \le \rho \le 1.1 \end{cases}$$

In comparison with the prototype test conducted by Huckert et al. (2016) [11], the discrete-element simulations of Villard et al. (2016) [2] for processes A and B, and the theoretical results of Lai (2018) [12] based on the partial soil-arching effect, the calculated results presented in this paper closely align with the prototype test outcomes of Huckert et al. (2016) [11], the simulation results of Villard et al. (2016) [2] for process A (as depicted in Figure 2), and the theoretical findings of Lai (2018) [12]. However, the settlement at the cavity centre due to the abrupt formation of the cavity was found to be less than the calculated results derived in this study.

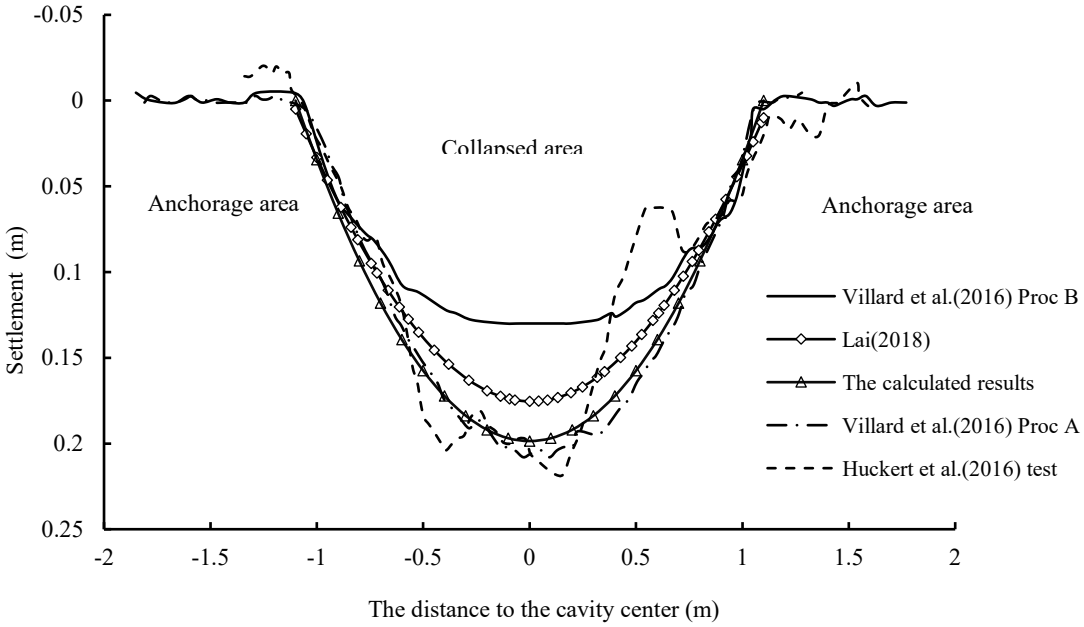

Figure 2. Comparison of the settlement results

Verification of Reinforced-Cushion Strain

Under conditions of large deformation, the radial strain of the thin circular plate is given by:

$$\varepsilon_\rho = \frac{du}{d\rho} + \frac{1}{2}\left(\frac{dw}{d\rho}\right)^2 \tag{3}$$

ε_ρ - radial strain (dimensionless).

The equations governing the radial displacement curve of the reinforced-cushion are presented as follows:

$$\begin{cases} u_1[\rho] = \left(-26.8 + 23.01\rho - 7.39\rho^2 + 1.05\rho^3 - 0.056\rho^4\right)\times 10^{-3} & 1.1 < \rho \le 4.4 \\ u_2[\rho] = \left(12.34\rho + 1.69\rho^2 - 18.58\rho^3\right)\times 10^{-3} & 0 \le \rho < 1.1 \end{cases}$$

The radial strain of the geosynthetic in both the anchorage and collapsed areas can be formulated as:

$$\begin{cases} \varepsilon_{\rho 1} = \left(23.01 - 14.77\rho + 3.15\rho^2 - 0.222\rho^3\right)\times 10^{-3} & 1.1 < \rho \le 4.4 \\ \varepsilon_{\rho 2} = \left(12.34 + 3.39\rho - 1.89\rho^2\right)\times 10^{-3} & 0 \le \rho \le 1.1 \end{cases}$$

Figure 3 illustrates the calculated strain results for the reinforced-cushion. When compared with the prototype test results from Huckert et al. (2016) [11], the numerical simulations for processes A and B by Villard et al. (2016) [2], and the calculation results by Lai (2018) [12] and Briancon et al. (2008) [8], the strain calculations from this study align well with the prototype test conducted by Huckert et al. (2016) [11]. The calculated values presented in this paper exceed those of the prototype test

and numerical calculations but are in close proximity to the findings of Briancon et al. (2008) [8]. The trend of radial strain variation in the reinforced-cushion, both in the anchorage area and the collapsed area, is fundamentally consistent with the outcomes obtained by the aforementioned methods. The radial strain of the reinforced-cushion is maximized at the cavity boundary, while the strain at the cavity's centre is significantly lower than that at its edge.

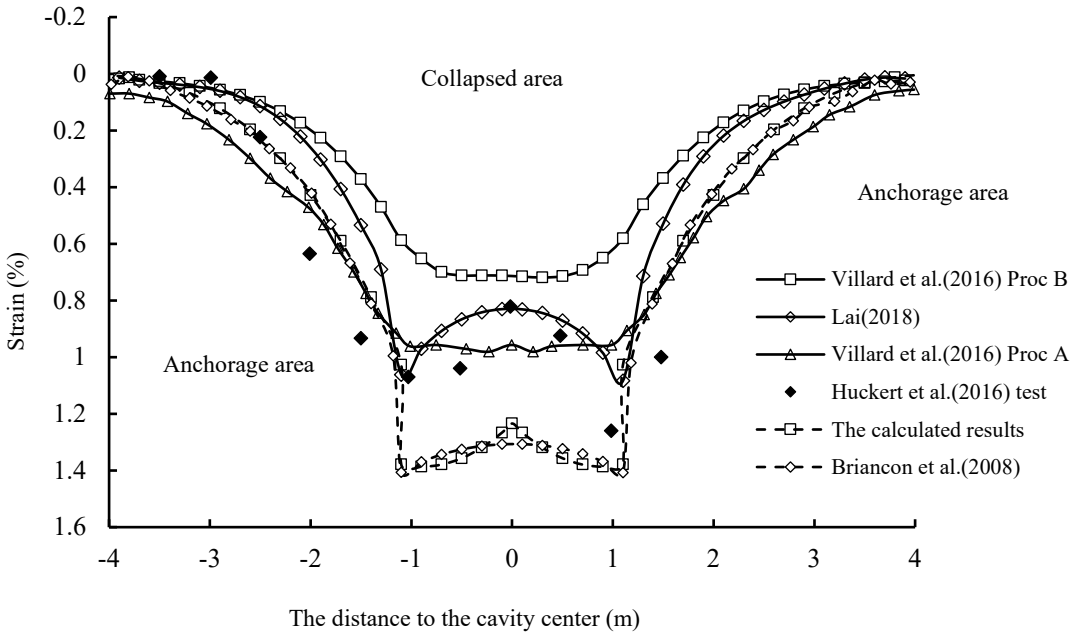

Figure 3. Comparison of the reinforcement strain results

INFLUENCE FACTORS ON THE DEFLECTION OF REINFORCED-CUSHION

The formation of cavities can result in uneven surface settlement, posing a threat to traffic safety. Consequently, it is essential to analyse the factors that influence the deflection of the reinforced-cushion, including the height of the embankment, parameters at the reinforcement-soil interface, the modulus of subgrade reaction, and the shear modulus of the foundation soil. The subsequent analysis employs dimensionless parameters to facilitate this examination.

Effect of Embankment Height

The height of the embankment directly influences the magnitude of the load exerted on the reinforced-cushion. According to Coulomb's law, the embankment height plays a pivotal role in determining the frictional resistance at the reinforcement-soil interface. In the calculations, it is assumed that the embankment fill parameters γ =19kN/m^3, φ =36°, c=0; the reinforcement-soil interface parameters φ_u =φ_l =25° , c_u =c_l =0, k_h^*=2000; the thickness of reinforced-cushion δ^*=0.003; the foundation parameters k_s^*=500, and $(GH)^*$=500. Calculate the deformations for the values of h^*=1,2,3,4.

In the field of road engineering, differential settlement is typically a greater concern than absolute settlement. Figure 4 illustrates the differential settlements at various distances from the cavity centre in relation to point B. Additionally, Figure 5 depicts the settlements at point B for different embankment heights. Taking into account the foundation settlement, the differential settlement progressively increases from the stable area towards the cavity's edges within the AB segment, a phenomenon not captured in previous studies. Therefore, it is essential to incorporate the settlement of the underlying foundation into the deformation analysis when examining the cavity development area.

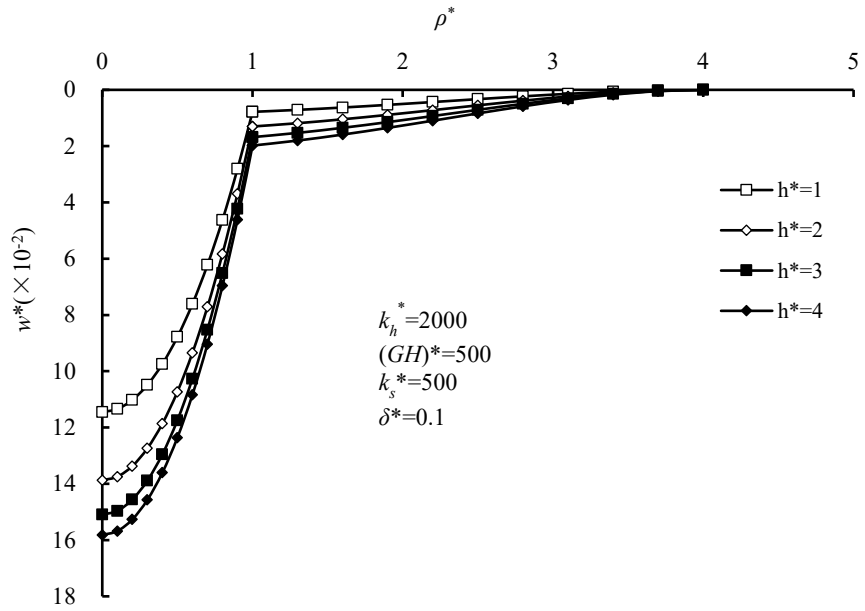

Figure 4. Effect of the embankment height on the reinforced-cushion settlement

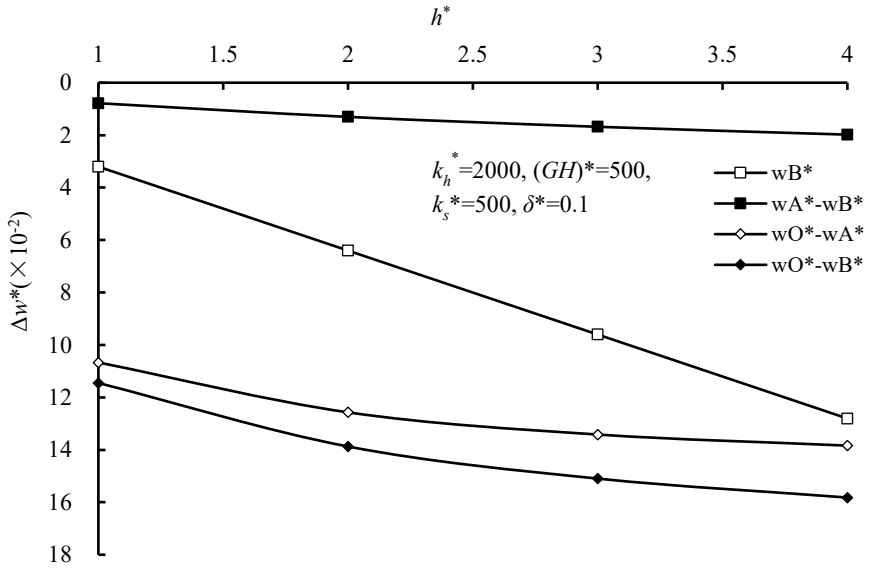

Figure 5. Effect of the embankment height on the differential settlement of the geogrid cushion

The differential settlement of the reinforced-cushion relative to point B escalates with the increment of h^*. However, as h^* increases, the growth rate of this differential settlement progressively diminishes because n decreases due to the soil arching effect.

Figure 5 depicts the settlement and differential settlement at three critical points: point O (the cavity centre), point A (the cavity boundary), and point B (the effect boundary). The maximum differential settlement was observed in the collapsed area, specifically within the OA segment. The analysis revealed that as h^* increases, both the settlement and differential settlement also increase. However, the rate at which the differential settlement grows diminishes over time. Notably, when the embankment height surpasses the cavity diameter, the impact of h^* on the differential settlement in the anchorage areas (AB segment) becomes minimal.

Effect of Reinforcement-Soil Interface Friction

This paper employs the tangential resistance coefficient at the reinforced cushion interface to analyse the impact of

reinforcement-soil interface friction, an approach suitable for scenarios where failure within the geosynthetic and the fill has not yet occurred. Figure 6 illustrates the differential settlement associated with varying tangential resistance coefficients at the reinforced cushion interface. The findings indicate that this coefficient predominantly influences the differential settlement relative to position A within the cavity, yet it does not affect the settlement value at point B or the differential settlement from the stable zone (location B) to the cavity's edge (location A). When the tangential resistance coefficient is zero, implying a smooth geosynthetic surface and neglecting the interface friction between the reinforcement and soil, the differential settlement in the collapsed area is at its maximum. However, as the tangential resistance coefficient increases, the influence of the interface strength between the reinforcement and soil on the differential settlement in the subsidence area diminishes gradually. Consequently, relying solely on increasing the friction at the reinforcement-soil interface to reduce settlement in the collapsed area is not a recommended strategy.

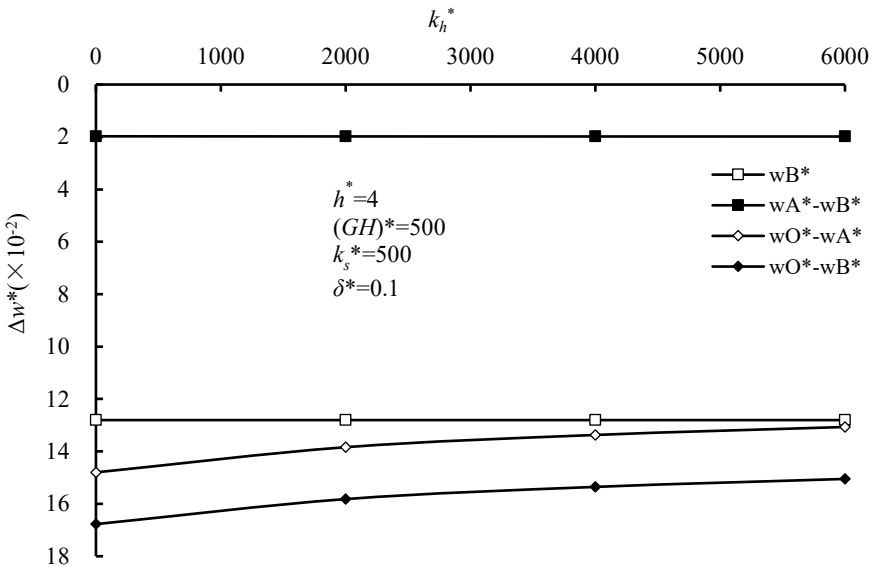

Figure 6. Effect of tangential resistance coefficient on differential settlement

Effect of the Modulus of Subgrade Reaction of the Pasternak Foundation

Given that the embankment fill parameters γ =19kN/m^3, and c=0, the embankment height h^* = 1, 4, k_h^*=2000, δ^*=0.1, and the foundation $(GH)^*$=500, the deformations of the reinforced-cushion corresponding to k_s^*=500, 1000, 1500, 2000,were calculated (Figure 7 and 8). An increase in k_s^* can mitigate the differential settlement relative to point B. However, when $k_s^* \geq$ 1500, further increments have a minimal impact on the differential settlement. Within the collapsed area, specifically the OA segment, an increase in k_s^* does not affect the differential settlement. Conversely, in the anchorage areas, denoted as the AB segment, an increase in k_s^* leads to a reduction in differential settlement. Therefore, the modulus of subgrade reaction of the Pasternak foundation predominantly influences the differential settlement outside the sinkhole, with no significant effect on the differential settlement within the cavity itself. As the embankment height increases, the influence of k_s^* on settlement becomes more pronounced.

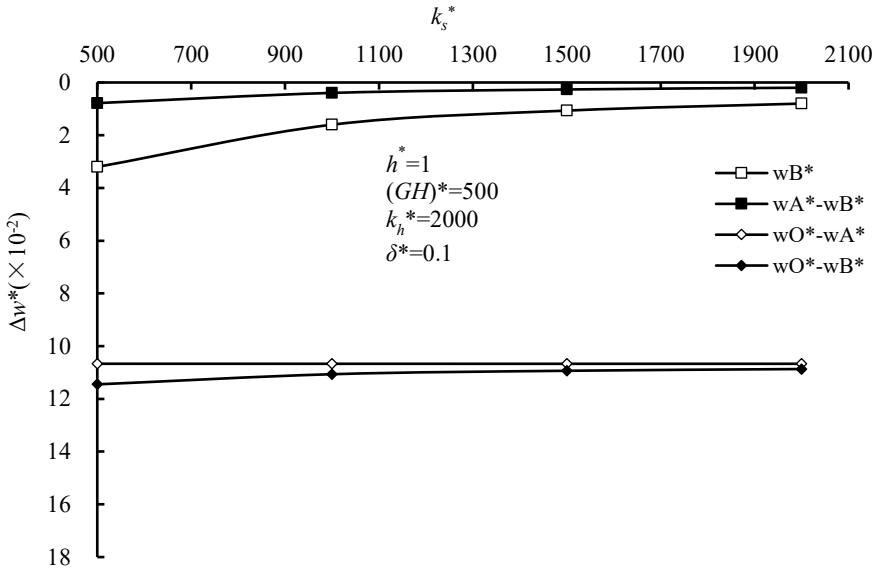

Figure 7. Effect of the modulus of subgrade reaction on the differential settlement of the geogrid cushion (h^* = 1)

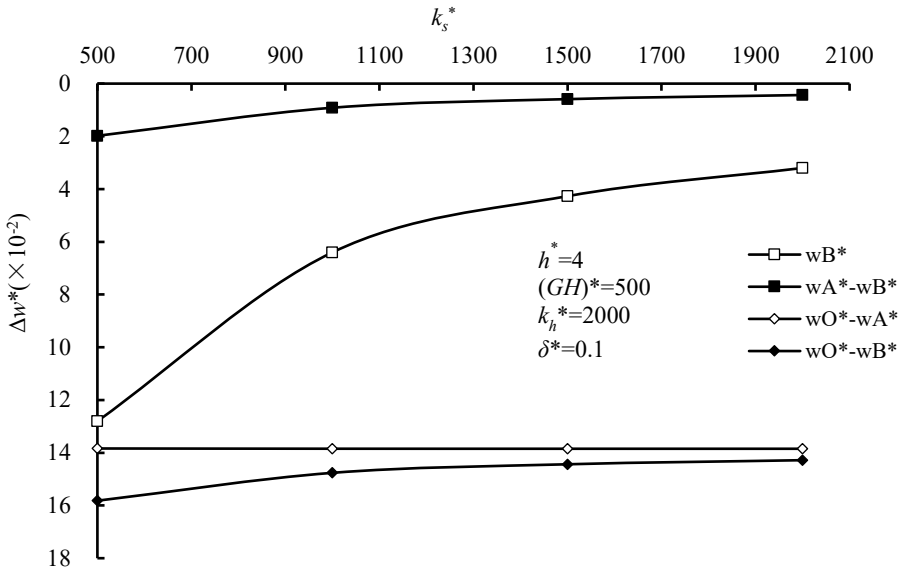

Figure 8. Effect of the modulus of subgrade reaction on the differential settlement of the geogrid cushion (h^* = 4)

Effect of Shear Modulus of the Pasternak Foundation

Regarding the modulus G, Tanahashi (2004) [30] suggested that when the Poisson's ratio of the soil is 0.35, a specific condition $\sqrt{k_s/G} = 5.4/H$ is met. Consequently, G can be ascertained based on k_s and H.

Figure 9 illustrates the differential settlement for various values of $(GH)^*$, with h^* = 4 and 6, k_s^* =300 and 500, respectively. The variation in $(GH)^*$ exerts no influence on the differential settlement within the collapse area (OA segment), but it primarily affects the differential settlement outside the cavity. As the $(GH)^*$ value increases, the differential settlement also increases, although the rate of this increase diminishes over time.

When the embankment height is relatively low (h^*=4), the load exerted on the reinforced cushion is minimal, resulting in a negligible effect of $(GH)^*$ on the deformation of the reinforced cushion; hence, $(GH)^*$ can be disregarded in the analysis. Conversely, when the embankment height is substantial (h^*=6), $(GH)^*$ significantly influences the differential settlement of the reinforced cushion, necessitating its inclusion in the analysis. Consequently, employing the Winkler foundation model to

analyse the deformation of geosynthetics in areas with high fill and cavity development can yield hazardous outcomes.

When the value of $(GH)^*$ is low, variations in filling heights exert minimal influence on the differential settlement within the anchorage zone (AB range). However, as the value of $(GH)^*$ increases beyond 1000, the impact on differential settlement becomes more pronounced. Additionally, despite differences in $(GH)^*$ at equivalent filling heights, the differential settlement in the collapse area (OA range) remains constant.

when k_s^* is small (k_s^* = 300), $(GH)^*$ exerts a relatively large influence on the differential settlement within the anchorage areas (AB segment), but has little effect in the collapsed area (OA segment). When k_s^* is held constant and H^* increases, both G^* and G^*H^* rise accordingly. With an increase in the shear modulus, the differential settlement in the anchorage areas (AB segment) also increases gradually.

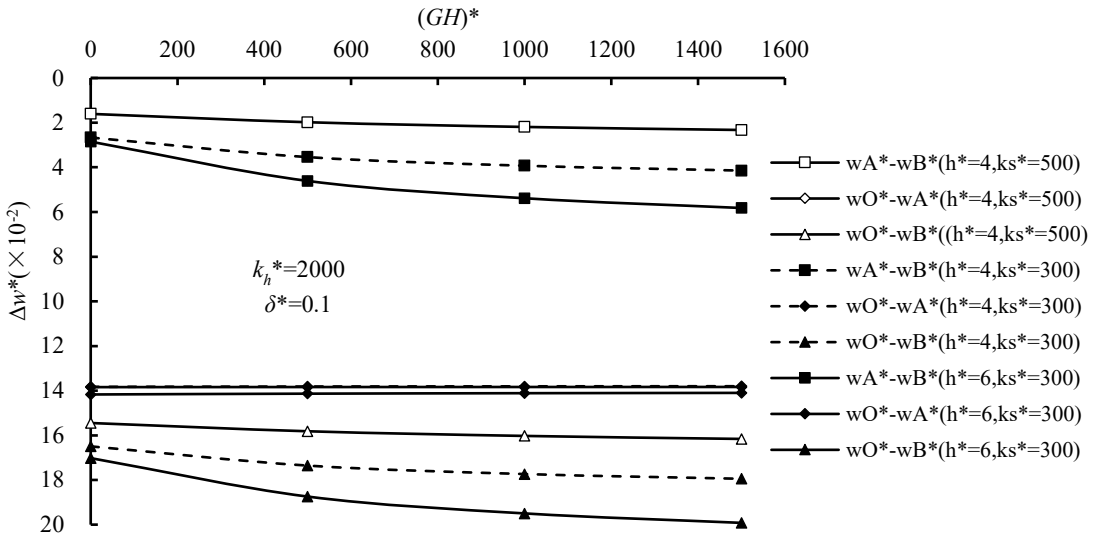

Figure 9. Effect of shear modulus on the differential settlement of the geogrid cushion

CONCLUSIONS

(1) This study posits that the foundation, cavity, and reinforced-cushion constitute a single entity, converting the self-weight of the embankment and geogrid-soil interfacial friction into an external load. Employing the principle of minimum potential energy, the analysis integrates three types of strain energy and external work, yielding a proposed analytical expression for geogrid cushion deformation. This method accounts for the foundation deformation conditions within the cavity development area.

(2) The settlement and differential settlement both escalate with increasing embankment height, yet the impact diminishes progressively. Once the embankment height surpasses the cavity diameter, the differential settlement in the anchorage areas is minimally affected by further height increases.

(3) When considering the interfacial friction of the reinforced cushion with a tangential resistance coefficient, an increment in this coefficient progressively attenuates its influence on the differential settlement within the subsidence area.

(4) In the anchorage areas, an increase in the modulus of subgrade reaction can mitigate the differential settlement relative to the stable area. Conversely, in the collapsed area, it exerts no influence on the differential settlement relative to the cavity's edges. With the increase in embankment height, the influence of the modulus of subgrade reaction on the settlement became more pronounced.

(5) In scenarios where the embankment height is substantial, the modulus of subgrade reaction is low, and the thickness of the shear layer is considerable, the shear modulus's impact on reinforced-cushion deformation must not be overlooked. Incorporating the shear modulus results in higher deflection values. However, the shear modulus exerts no influence on the differential settlement relative to the cavity's edges in the collapsed area.

ACKNOWLEDGEMENTS

The author would like to express her special appreciation to the anonymous reviewers for their valuable comments and suggestions. This work is supported by the Natural Science Foundation of Fujian Province (Grant No. 2021J01338), the Transportation Science and Technology Project of Fujian Provincial Department of Communications (Grant No. 202032), Fujian Chuanzheng Communications College Technology Service Projects (Grant No. CZJTJGX20180006), and the Science and Education Development Fund of Fujian Chuanzheng Communications College (Grant No.20220202).

REFERENCE

[1] Wang K., Zhang J., Gao G., et al. 2022. Causes, risk analysis, and counter-measures of urban road collapse in China from 2019 to 2020. Journal of Performance of Constructed Facilities 36(6): 40-54.

[2] Villard P, Huckert A, Briançon L., 2016. Load transfer mechanisms in geotextile-reinforced embankments overlying voids, Numerical approach and design. Geotextiles and Geomembranes 44(3), 381-395.

[3] Wu D., Wu J., Xu C., et al. 2020. Model test of geotextiles in controlling the collapse of karst roadbed. Rock and Soil Mechanics, 41: 1−11. (In Chinese)

[4] Zornberg J G, Roodi G H. Use of geosynthetics to mitigate problems associated with expansive clay subgrades. Geosynthetics International, 2021, 28(3): 279−302.

[5] Giroud J P, Bonaparte R, Beech J F. 1990. Design of Soil Layer-Geosynthetic Systems Overlying Voids. Geotextiles and Geomembranes, 9,11-50.

[6] Wang M C, Feng Y X, Jao M., 1996. Stability of geosynthetic-reinforced soil above a cavity. Geotextiles & Geomembranes 14(2), 95-109.

[7] Briancon L, Villard P.,2008. Design of geosynthetic-reinforced platforms spanning localized sinkholes. Geotextiles and Geomembranes 26(5), 416-428.

[8] Villard P, Briancon L., 2008. Design of geosynthetic reinforcements for platforms subjected to localized sinkholes. Canadian Geotechnical Journal 45(2), 196-209.

[9] Le V, Huang J, Bin-Shafique S., 2014. Model Tests of Subsidence of the Reinforced Soil over Void. Ground Improvement and Geosynthetics, Shanghai, CHN, 312-321.

[10] Van Dyk C, Jacobsz S W., 2016 The Behaviour of a Reinforced Soil Mattress Spanning a Cavity Modelled in a Geotechnical Centrifuge. Geotechnical and Geological Engineering 34(5), 1345-1358.

[11] Huckert A, Briançon L, Villard P., 2016. Load transfer mechanisms in geotextile-reinforced embankments overlying voids: Experimental and analytical approaches. Geotextiles and Geomembranes 44(3), 442-456.

[12] Lai F., 2018. Load transfer mechanisms and design method of low geosynthetic-reinforced embankment (LGR) subjected to localized voids. M.S. Thesis, Fuzhou University, Fuzhou, CHN. 79-89. (In Chinese)

[13] Wang Z., Gao G., Yang G., et al. 2024.Mesoscopic study on mechanical behavior evolution and deformation mechanism of overlying reinforced subgrade in subsidence area. Journal of Central South University (Science and Technology) 55(4), 1523-1536. (In Chinese)

[14] Zheng J., Zhang J., Ma Q., 2010. Three-dimensional analysis of pile-earth stress ratio of biaxial reinforcement composite foundation. J. Huazhong Univ. of Sci. & Tech. (Natural Science Edition) 38(2), 83-86. (In Chinese)

[15] Calio I, Greco A.,2013. Free vibrations of Timoshenko beam-columns on Pasternak foundations. Journal of Vibration & Control 19(5), 686-696.

[16] Zhao L, Zhou W. Fatahi B., 2016. A Dual Beam Model for Geosynthetic- Reinforced Granular Fill on an Elastic Foundation. Applied Mathematical Modelling 40(21-22), 9254-9268.

[17] M E.,1999. Fundamental frequencies of Timoshenko beams mounted on Pasternak foundation. Journal of Sound & Vibration 228(2),452-457.

[18] Khajeansari A, Baradaran G H, Yvonnet J.,2012. An explicit solution for bending of nanowires lying on Winkler–Pasternak elastic substrate medium based on the Euler–Bernoulli beam theory. International Journal of Engineering Science52(3), 115-128.

[19] Yu H, Cai C, Yuan Y., 2017. Analytical solutions for Euler-Bernoulli Beam on Pasternak foundation subjected to arbitrary dynamic loads. International Journal for Numerical & Analytical Methods in Geomechanics 41(8), 1125-1137.

[20] Wu F., Chen Z., Deng Y., 2024. Solution of double beam model for deformation of reinforced roadbed with shallow soil hole. Engineering Journal of Wuhan University 57(5), 593-600. (In Chinese)

[21] Bian X. Song Guang, Chen Yunmin, 2012. Deformation behaviours of geogrid reinforcement in Pasternak ground. Engineering Mechanics 29(5), 147-155. (In Chinese)

[22] Güler K., 2004. Circular elastic plate resting on a tensionless Pasternak foundation. Journal of Engineering Mechanics 130(10), 1251-1254.

[23] Shukla S K, Gupta A, Sivakugan N., 2011. Analysis of Circular Elastic Plate Resting on Pasternak Foundation by Strain Energy Approach. Geotechnical and Geological Engineering 29(4), 613-618.

[24] Jones B M, Plaut R H, Filz G M.,2010. Analysis of geosynthetic reinforcement in pile-supported embankments. Part I: 3D plate model. Geosynthetics International 17(2), 59-67.

[25] Zhao M., Liu M., Ma B., 2016. Calculation for Stress Concentration Ratio and Settlement of Bidirectional Reinforced Composite Foundation Consisting of Geogrid Mattress and Stone Column Under Embankment. China Journal of highway transport 29(5), 1-10. (In Chinese)

[26] Adachi T, Kimura M, Kishida K, 2003. Experimental study on the distribution of earth pressure and surface settlement through three-dimensional trapdoor tests. Tunnelling and Underground Space Technology 18(2-3),171-183.

[27] Blight G, Barrett A. ,1990. Field test of catenary net to protect traffic from mining subsidence. Journal of Transportation Engineering 116(2), 135-144.

[28] Espinoza R D, Bray J D., 1995. An integrated approach to evaluating single-layer reinforced soils. Geosynthetics International 2(4), 723-739.

[29] He W., Li K., Wang F., 2016. Large-scale experimental study of multi-layered reinforcement to prevent underneath sinkhole in karst terrain and the design method. Chinese Journal of Rock Mechanics and Engineering, 35(5), 980-988. (In Chinese)

[30] Tanahashi H., 2004. Formulas for an Infinitely Long Bernoulli-Euler Beam on the Pasternak Model. Soils and Foundations, 44(5), 109-118.